Front. Earth Sci. 2023, 17(1): 121−134
https://doi.org/10.1007/s11707-022-0974-y

RESEARCH ARTICLE

Coalbed methane desorption characteristics controlled by coalification and its implication on gas co-production from multiple coal seams

Bin ZHANG[1,2], Yafei ZHANG[3], Suping ZHAO[4], Wei HE[5], Shu TAO (✉)[1,2], Zhejun PAN[6], Yi CUI[7]

1 School of Energy Resources, China University of Geosciences (Beijing), Beijing 100083, China
2 Coal Reservoir Laboratory of National Engineering Research Center of CBM Development & Utilization, Beijing 100083, China
3 China United Coalbed Methane Corporation Ltd., Beijing 100016, China
4 PetroChina Research Institute of Petroleum Exploration and Development, Beijing 100083, China
5 Ningxia Mineral Geological survey Institute, Yinchuan 750021,China
6 Key Laboratory of Continental Shale Hydrocarbon Accumulation and Efficient Development (Ministry of Education), Northeast Petroleum University, Daqing 163318, China
7 China Huaneng Group, Beijing 100031, China

Abstract In this work, CH_4 isothermal adsorption measurements were carried out on 64 coal samples collected from western Guizhou Province of China, and the coalbed methane (CBM) desorption processes were quantitatively analyzed. The results show that the Langmuir volume and the Langmuir pressure are controlled by coalification, and tend to increase as the vitrinite reflectance changes from 0.98% to 4.3%. Based on a division method of CBM desorption stages, the CBM desorption process were divided into four stages (inefficient, slow, fast and sensitive desorption stages) by three key pressure nodes (the initial, turning and sensitive pressures). The fast and sensitive desorption stages with high desorption efficiency are the key for achieving high gas production. A theoretical chart of the critical desorption pressure (P_{cd}) and its relationship with different pressure nodes was established. The higher-rank coals have the higher initial, turning and sensitive pressures, with larger difference between pressure nodes. Most CBM wells only undergo partial desorption stages due to the differences in P_{cd} caused by the present-gas content. Under the same gas content conditions, the higher the coal rank, the less desorption stages that CBM needs to go through. During coalbed methane co-production from multiple coal seams within vertically superposed pressure systems, the reservoir pressure, the P_{cd}, the initial working liquid level (WLL) height, and coal depth are key factors for evaluating whether coal seams can produce CBM simultaneously. It must be ensured that each production layer enters at least the fast desorption stage prior to that the WLL was lower than the depth of each layer. Only on this basis can all layers achieve the maximum gas production.

Keywords co-production from multiple coal seams, CBM, adsorption, desorption, coal rank

Received December 24, 2021; accepted February 14, 2022

E-mail: taoshu@cugb.edu.cn

1 Introduction

In China, commercial development of coalbed methane (CBM) has been achieved in the Qinshui and Ordos Basins with progress in the Junggar Basin (Li et al., 2019; Tao et al., 2019a, 2019b; Chen et al., 2021a). In recent years, the resources within multiple (> 20 seams) and thin (generally less than 2 m in thick) seams in the south China have received attention (Qin et al., 2018a). CBM resource is relatively small in each coal seam due to limited coal thickness, and CBM co-production is considered as the best development mode to achieve economic benefit (Beaton et al., 2006; Xu et al., 2016; Wu et al., 2018; Yang et al., 2018b). The main challenges in advancing the state of the science and resource development in rationalization of the complex geology and multiple coal seams contributions from geological perspectives (Qin et al., 2008; Shen at al., 2016; Wang and Qin, 2019; Zhang et al., 2019; Chen et al., 2021b, 2016c; Zhao et al., 2021). One of the current challenges is the lack of feasibility evaluation method for the layer

combination, especially for areas with different coal rank and vertically superposed pressure systems (Chen et al., 2017, 2018). During co-production from multiple coal seams, the CBM in each layer will desorb in turn as the working liquid level (WLL) height and bottom hole flow pressure (BHFP) drop. Therefore, the desorption behavior of each seam plays an important role in the dynamic process of co-production, which is directly related to the feasibility of the layer's combination. Several studies found that it is critical that the WLL is above the depth of the layer before CBM is desorbed (Yang et al., 2018a). Only in this case can all productive layers produce gas. However, the gas desorption is a nonlinear process in which the desorption efficiency changes dynamically as pressure changes (Meng et al., 2015; Xu et al., 2021).

Based on the Langmuir isotherm adsorption theory (Langmuir, 1916), the three key pressure nodes (the initial, turning and sensitive pressures) determined by the desorption curvature on the adsorption isotherm divide the desorption process into four stages (inefficient, slow, fast and sensitive desorption stages) by Meng et al. (2014). The difference in desorption efficiency at different stages possesses different productivity. Fast and sensitive desorption stages at the early production stage are the key to achieve high-yield of CBM wells. The inefficient and slow desorption stages contribute little to the gas production. Further refinement of the desorption characteristics of different coal seams is of great significance for the optimization of the co-production layer combination in multi- and thin- seam area.

In this work, the isothermal adsorption experiments were conducted on 64 samples with vitrinite reflectance (R_o) of 0.98%–4.3% from western Guizhou Province, and the CBM desorption process was quantitative analyzed. The methane adsorption and desorption characteristics controlled by the coalification were investigated. Furthermore, the theoretical investigation on the dynamic process of CBM co-production from multiple coal seams was presented, and the implication of the division of desorption stages on CBM development was discussed. As a result, a feasibility evaluation method for the layer combination was established to guide effective gas extraction in similar areas.

2 Sample preparation and experiments

Coal-bearing sequences were deposited in the Longtan Formation and Changxing Formation of Late Permian in western Guizhou Province (Fig. 1(a)) (Dai et al., 2005; Ren et al., 2018). The coal bearing strata deposited in transitional facies consisting of tight sandstone, siltstone, silty mudstone, limestone, mudstone and coal seams. Despite the large-scale development of marshes in the area, the stable period of peat swamps is short due to the influence of high-frequency sea level changes, resulting in a wide distribution of multiple coal seams with thin thickness in each layer (> 20 seams, generally less than 2 m in thickness) (Shen et al., 2016). Varying magma intrusion in the mid-Yanshanian Period caused the current distribution of coal rank with R_o ranging from 0.7% to 4.5% (Chen et al., 2018). Coal samples with a depth of 158–1016 m in this work are drilling coal cores from 11 CBM wells (Fig. 1(b); Table 1) in Panguan (Well 1, 4), Tucheng (Well 3), Zhuzang (Well 11), Santang (Well 10), Bide (Well 5,6,7), Qianxi (Well 9) and Dahebian synclines (Well 2). Well 8 located in Laochang Block of eastern Yunnan Province. Based on ISO 7404.3-1994 and ISO 7404.5-1994, mean R_o were measured using a Leitz MPV-3 photometer microscope. The isothermal adsorption experiments were conducted using a USA Terratek Isotherm Measurement System (ISO-300), under the condition of equilibrium pressure at 5–12 MP. Here the influence of temperature was not considered, and thus the temperature of all measurements was set to 30°C before test. All the samples were crushed and sieved to a size of 0.18–0.25 mm (60–80 mesh), and then sent for moisture-equilibrium treatment for at least 48 h.

3 Division of CBM desorption stages

The division of CBM desorption stages was based on the mathematical curvature of the adsorption isotherms. The details for the derivation process were presented by Meng et al. (2014). Here, the desorption efficiency (D_e, $m^3 \cdot t^{-1} \cdot MPa^{-1}$) is defined as the desorbed gas volume per tonne of coal under unit pressure drop, which represents the first derivative of adsorption capacity according to Langmuir equation (Fig. 2):

$$D_e = V' = \frac{V_L P_L}{(P + P_L)^2} = \frac{A^2}{B^2}, \tag{1}$$

where V' represents adsorption capacity, m^3/t; V_L represents Langmuir volume, m^3/t; P_L represents Langmuir pressure, MPa; P represents the reservoir pressure, MPa; $A = \sqrt{V_L P_L}$; $B = P + P_L$.

The desorption efficiency of coalbed methane increases with the decrease of reservoir pressure. The curvature is used to quantitatively characterize the bending deformation degree of the desorption curve (Fig. 2) (Department of Applied Mathematic Tongji University, 2002). According to the mathematical expression of curvature, the curvature (D_c) of the CBM desorption curve is expressed as

$$D_c = \frac{|V''|}{(1+V'2)^{3/2}} = \frac{\left| -\frac{2V_L P_L}{(P+P_L)^3} \right|}{\left(1 + \left(\frac{V_L P_L}{(P+P_L)^2}\right)^2\right)^{3/2}} = \frac{2A^2/B^3}{(1+A^4/B^4)^{3/2}}. \tag{2}$$

With decreasing pressure, the D_c exhibits a change

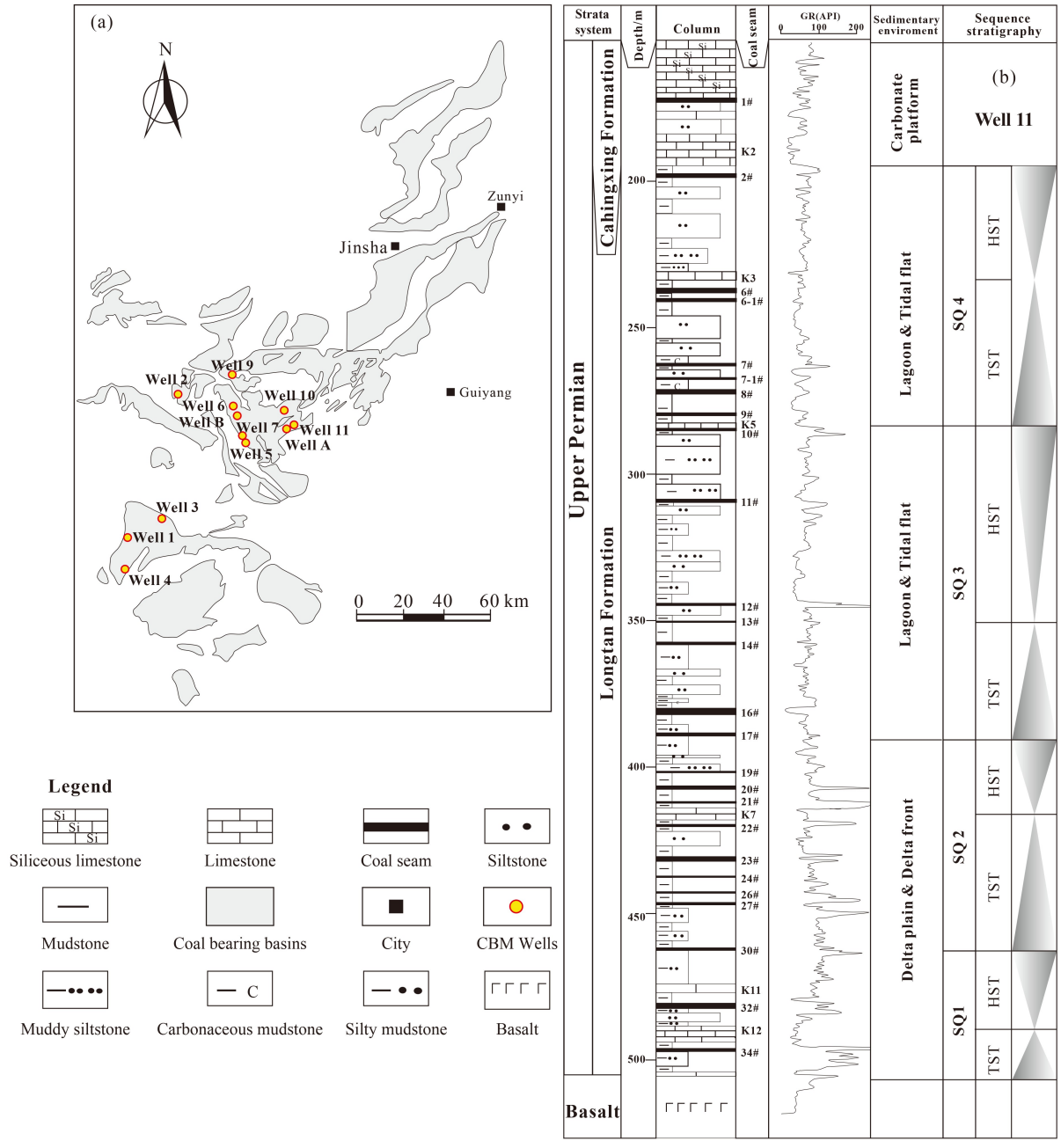

Fig. 1 (a) Distribution of coal-bearing basins and CBM wells in the western Guizhou Province; (b) stratigraphic column and sedimentary characteristics of the coal-bearing strata of well 11.

trend of slowly increases → rapidly increases → rapidly decreases → slowly decreases in sequence. Here, the first derivative of D_c is characterized as

$$D'_c = 6A^2B^{-8}\left(1+A^4B^{-4}\right)^{-5/2}(A^4-B^4). \quad (3)$$

When the D_c reaches the maximum value, D'_c equal to 0. And the corresponding reservoir pressure (P_t, turning pressure) is

$$P_t = \sqrt{V_L P_L} - P_L. \quad (4)$$

Its mathematical significance is that the desorption efficiency begins to increase significantly when the reservoir pressure drops to the turning pressure. Then, the second derivative of D_c is further expressed as

$$D''_c = 12A^2B^{-13}\left(1+A^4B^{-4}\right)^{-7/2}(A^8-7A^4B^4+2B^8). \quad (5)$$

There are two inflection points in the desorption curve which make the $D''_c = 0$, indicating two pressure points at which the growth rates of desorption efficiency changes significantly. The corresponding pressures are characterized by the starting pressure (P_i) and sensitive pressure

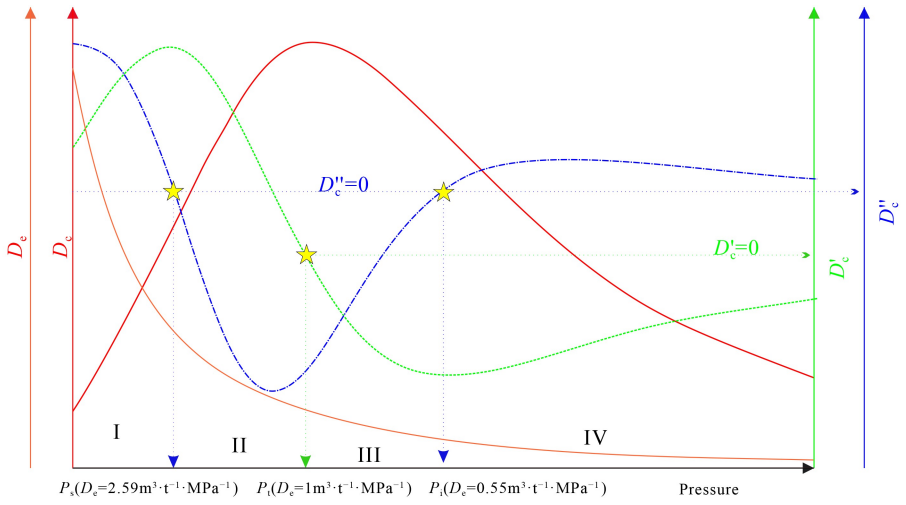

Fig. 2 The division of desorption stages using the mathematical curvature.

(P_s), respectively:

$$P_s = \left(\frac{7-\sqrt{41}}{4}\right)^{1/4} \times \sqrt{V_L P_L} - P_L, \quad (6)$$

$$P_i = \left(\frac{7+\sqrt{41}}{4}\right)^{1/4} \times \sqrt{V_L P_L} - P_L. \quad (7)$$

The D_e values corresponding to P_i, P_t, and P_s are 0.55 $m^3/(t{\cdot}MPa)$, 1.00 $m^3/(t{\cdot}MPa)$ and 2.59 $m^3/(t{\cdot}MPa)$, respectively. Based on these three pressure nodes, the CBM desorption curve can be divided into inefficient ($P \geqslant P_i$, $D_e \leqslant 0.55$ $m^3{\cdot}t^{-1}{\cdot}MPa^{-1}$), slow ($P_i < P \leqslant P_t$, $0.55 < D_e \leqslant 1$ $m^3{\cdot}t^{-1}{\cdot}MPa^{-1}$), fast ($P_t < P \leqslant P_s$, $1 < D_e \leqslant 2.59$ $m^3{\cdot}t^{-1}{\cdot}MPa^{-1}$), and sensitive ($P > P_s$, $D_e > 2.59$ $m^3{\cdot}t^{-1}{\cdot}MPa^{-1}$) desorption stages (Fig. 2). Different stages have different desorption efficiency and different productivity.

4 Experimental results and discussion

4.1 Langmuir pressure and volume variations with coal rank

The V_L of 64 samples in this work ranges from 3.77 m^3/t to 39.32 m^3/t, with an average of 21.33 m^3/t; The P_L varies over a wide range between 0.35 MPa and 2.76 MPa, averaging at 1.8 MPa (Table 1). There is small difference in V_L and P_L for different coal seams in the same well, with the biggest differences change from 1.1 m^3/t to 5.19 m^3/t (averaging at 2.62 m^3/t) and 0.15–0.73 MPa (averaging at 0.37 MPa). This is also supported by Chen et al. (2018) that the adsorption capacity of coal reservoirs in the same well were similar because of the similar coal maturity. The Langmuir parameters between different wells various greatly (Fig. 3), with the mean value of V_L ranges from 4.86 m^3/t to 36.11 m^3/t. For example, the V_L and the P_L of coal seam No. 7 in well 1 is only 5.27 m^3/t and 0.98 MPa, respectively, while those in well 11 reach 37.08 m^3/t and 2.76 MPa.

There are many factors affecting the CBM adsorption and desorption behaviors, including coalification, material composition, pressure, and temperature (Crosdale et al., 1998; Wu et al., 2017; Mohanty et al., 2018; Tao et al., 2018). In generally, coal rank and pressure have a positive effect on coal adsorption capacity, while the moisture content and temperature play a negative role. Here, coal rank is the most important factor for the difference of test parameters between different wells. Figure 3 illustrates the relationships between V_L, P_L, and R_o. The results show that lower-rank coals have a lower value of V_L and P_L, while higher-rank coals exhibit strong adsorption capacity. High P_L suggests that high rank coals saturate at higher pressure. For coal reservoirs with R_o from 0.98% to 3%, both V_L and P_L increase linearly as coal rank increases. When the R_o is greater than 3.0%, there is a slow increase trend in V_L and a small change range in P_L as the R_o further increases. The main reason for the change of Langmuir parameters is the variation of pore size distribution caused by coalification. Numerous studies suggested that ISSA of coal reservoirs varies with the R_o in a similar trend (Nie et al., 2015; Zhao et al., 2016; Li et al., 2017; Chen et al., 2017). Generally, the micropores are abundant in high-rank coals, providing more available sites for CH_4 adsorption than that of lower rank coals. According to Fig. 3, the relevant relationships between R_o, V_L and P_L can be expressed as follows:

$$P_L = -0.1988R_o^2 + 1.6206R_o - 0.6662 \quad (0.98\% \leqslant R_o \leqslant 4.3\%)\ R^2 = 0.92, \quad (8)$$

$$V_L = -2.017R_o^2 + 20.55R_o - 12.841 \quad (0.98\% \leqslant R_o \leqslant 4.3\%)\ R^2 = 0.95. \quad (9)$$

Table 1 The Langmuir parameters and key pressure nodes of 64 coal samples

Well	Seam No.	R_o/%	Depth/m	Langmuir volume /($m^3 \cdot t^{-1}$)	Langmuir pressure /MPa	Sensitive pressure /MPa	Turning pressure /MPa	Starting pressure /MPa
Well 1	4#	0.98	661.36	4.54	0.71	0.41	1.09	1.72
	7#	1.00	687.01	5.62	0.98	0.48	1.37	2.20
	10#	1.02	706.17	3.77	0.63	0.33	0.91	1.46
	18#	1.04	774.83	5.27	0.80	0.48	1.25	1.98
	19#	1.08	793.83	5.02	1.01	0.39	1.24	2.03
	24#	1.20	833.82	4.61	0.77	0.40	1.11	1.78
	30#	1.24	882.23	5.20	1.00	0.42	1.28	2.09
Well 2	3#	1.12	/	8.84	0.83	0.85	1.88	2.84
	5#	1.08	/	6.83	0.57	0.66	1.41	2.11
	6#	1.15	/	8.93	0.86	0.86	1.91	2.89
	7#	1.09	843.90	8.26	0.79	0.80	1.76	2.66
	9#	1.07	854.30	5.82	0.35	0.54	1.07	1.58
Well 3	5_2#	1.38	643.83	14.67	1.41	1.42	3.14	4.74
	9#	1.40	661.98	16.36	1.55	1.58	3.49	5.26
	10#	1.44	676.77	15.99	1.62	1.54	3.47	5.26
	12#	1.42	705.35	14.13	1.62	1.35	3.17	4.86
	13#	1.47	722.09	14.69	1.24	1.41	3.03	4.53
	21#	1.55	839.69	13.84	1.27	1.34	2.92	4.40
	24#	1.58	901.27	16.58	1.70	1.60	3.61	5.49
	27_1#	1.67	920.71	14.63	1.91	1.38	3.38	5.24
	29_3#	1.69	955.97	15.23	1.40	1.47	3.21	4.84
Well 4	1#	1.78	536.88	19.67	1.69	1.89	4.08	6.11
	3#	1.79	559.68	20.98	1.97	2.03	4.46	6.73
	7#	1.92	581.48	20.23	1.70	1.94	4.16	6.23
	10#	1.98	612.28	21.26	1.55	2.02	4.19	6.22
Well 5	2#	2.06	856.25	19.65	1.54	1.88	3.96	5.90
	6#	1.93	916.70	20.41	1.77	1.97	4.24	6.36
	6#	2.12	920.40	20.00	1.68	1.92	4.12	6.16
	6#	2.24	917.00	21.55	1.75	2.07	4.39	6.56
	6#	2.08	918.30	21.41	1.73	2.05	4.36	6.50
	6#	2.00	921.40	21.55	1.59	2.05	4.26	6.33
Well 6	3#	1.80	639.10	19.91	1.81	1.92	4.19	6.31
	5#	1.90	661.20	19.84	1.78	1.91	4.16	6.26
	32#	2.20	898.40	22.27	1.93	2.14	4.63	6.94
	33#	2.30	921.10	21.02	1.88	2.03	4.41	6.63
Well 7	6#	2.00	638.00	22.37	1.82	2.15	4.56	6.81
	10#	2.39	836.80	23.04	1.95	2.22	4.75	7.12
	11#	2.36	839.48	23.26	1.78	2.22	4.65	6.93
	12#	2.42	855.40	22.16	2.02	2.14	4.67	7.03
Well 8	7-1#	2.69	886.33	24.46	1.86	2.33	4.89	7.27
	7-2#	2.69	887.15	25.66	2.12	2.46	5.26	7.86
	7-3#	2.68	887.66	25.51	1.86	2.42	5.03	7.46
	7-4#	2.58	888.34	25.33	1.92	2.41	5.05	7.52

(*continued*)

Well	Seam No.	R_o/%	Depth/m	Langmuir volume /($m^3 \cdot t^{-1}$)	Langmuir pressure /MPa	Sensitive pressure /MPa	Turning pressure /MPa	Starting pressure /MPa
	8-1#	2.69	922.95	26.31	2.20	2.53	5.41	8.09
	8-2#	2.74	923.50	26.01	2.48	2.51	5.55	8.39
	9-1#	2.74	955.23	25.99	2.49	2.51	5.55	8.39
	9-2#	2.78	955.70	26.25	2.35	2.53	5.50	8.28
	13-2#	2.85	992.20	27.76	2.42	2.67	5.78	8.67
	13-3#	2.83	993.25	28.11	2.59	2.71	5.94	8.95
	13-4#	2.85	994.30	28.29	2.26	2.71	5.74	8.56
	16-1#	2.85	1016.00	28.61	2.51	2.76	5.96	8.96
Well 9	4#	3.20	158.00	33.36	2.44	3.17	6.58	9.77
	9#	3.40	214.20	32.03	2.61	3.07	6.53	9.76
	10#	3.60	359.40	34.31	2.55	3.26	6.80	10.11
Well 10	6#	3.04	616.31	33.52	2.57	3.20	6.71	9.99
	7#	3.14	638.25	37.20	2.41	3.47	7.06	10.40
	14#	3.25	689.62	34.72	2.75	3.32	7.02	10.47
	14#	3.36	700.51	35.94	2.45	3.38	6.93	10.25
	16#	3.08	737.35	36.01	2.51	3.40	7.00	10.35
Well 11	2#	3.31	198.22	34.13	2.67	3.26	6.88	10.25
	6#	3.44	241.51	35.41	2.75	3.38	7.12	10.60
	7#	3.59	262.83	37.08	2.76	3.53	7.36	10.93
	16#	4.30	381.80	34.61	2.55	3.29	6.84	10.16
	23#	4.19	432.00	39.32	2.49	3.66	7.40	10.90

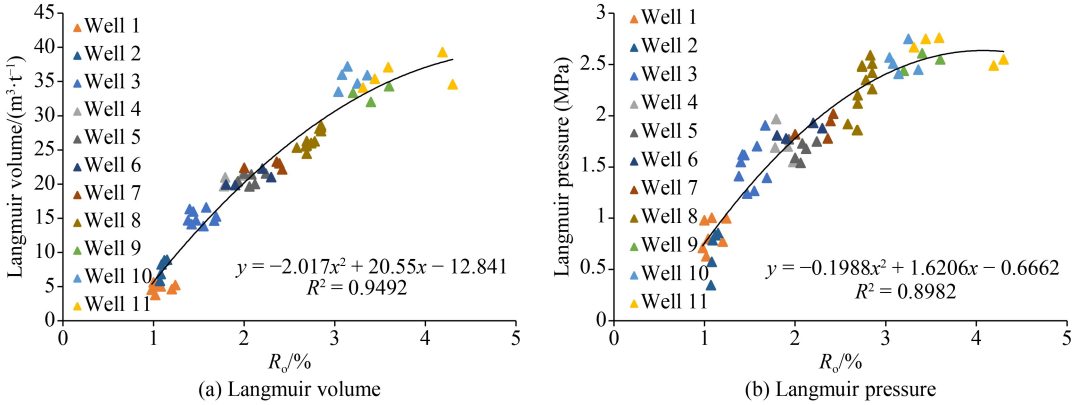

(a) Langmuir volume (b) Langmuir pressure

Fig. 3 The correlations between R_o, V_L, and P_L.

Moreover, the difference in adsorption capacity can also be reflected by the curve shapes. The isothermal adsorption curves of four typical coal samples are presented in Fig. 4. For coals with R_o of 0.98% and 1.98%, the adoption capacity increases slowly at low pressure and tend to be stable at 3 MPa and 5 MPa, respectively. For coals with R_o of 3.14% and 4.19%, there are no obvious difference in curve shape when pressure is less than 5 MPa. At high pressure zone (> 5 MPa), the adsorption capacity of coal with R_o of 3.14% is slightly higher than that of coal with R_o of 4.19%. In other words, when R_o < 3%, the difference in adsorption behavior of different rank coals is mainly from the low-pressure zone. As coal rank further increases, the difference is mainly manifested in the high-pressure zone.

4.2 Desorption efficiency and desorption stages

According to Eq. (1), the desorption efficiency of the

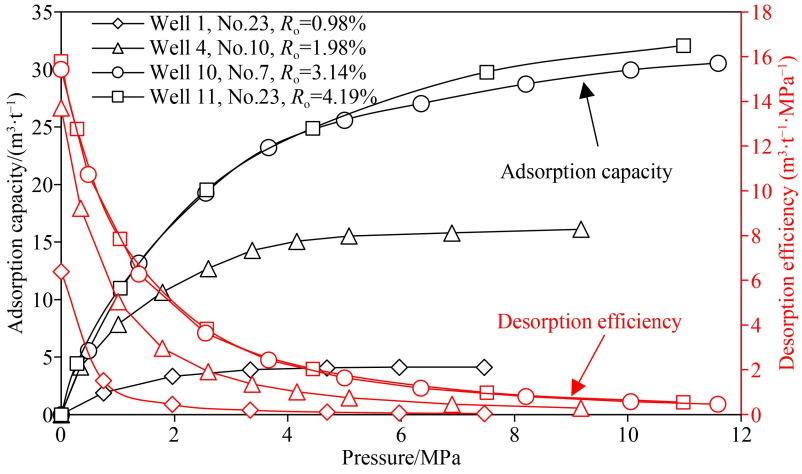

Fig. 4 CH_4 adsorption isotherm and desorption efficiency curves of 4 typical coal samples.

tested samples at different reservoir pressures can be obtained, as shown in Fig. 4. As the pressure decreases, the CBM desorption efficiency increases exponentially. At high reservoir pressure zone, the corresponding desorption efficiency is substantially constant or slowly increases. When the reservoir pressure drops to 0 MPa, the coal reservoir reaches the highest desorption efficiency (5–11 $m^3 \cdot t^{-1} \cdot MPa^{-1}$). Also, the desorption efficiency varies greatly between different rank coals. Taking the sample with R_o of 0.98% as example, the desorption efficiency begins to increase rapidly only when the pressure is less than 2 MPa. For coals with R_o of 3.14% and 4.19%, the desorption efficiency starts to increase rapidly at a pressure of about 4 MPa. Under the same pressure conditions, the desorption efficiency of higher rank coals is greater than the lower rank coals, especially in the low-pressure zone (Fig. 5).

To further characterize the desorption stages of different rank coals, the starting, turning and sensitive pressures are calculated based on Eq. (7), Eq. (6) and Eq. (4), respectively. The starting pressure of the 64 samples is between 1.46 MPa and 10.93 MPa, with an average of 6.55 MPa. The turning pressure ranges from

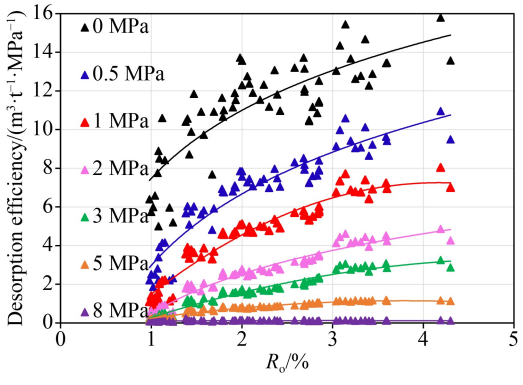

Fig. 5 The desorption efficiency of different rank coals under different reservoir pressure.

0.91 MPa to 7.4 MPa (with a mean of 4.37 MPa). The sensitive pressure varies from 0.33 MPa to 3.66 MPa, averaging at 2.03 MPa. Based on the three pressure nodes, the CBM desorption process is divided into four stages (Fig. 6). For coals with R_o of 0.98%, the starting, turning and sensitive pressures are 1.72 MPa, 1.09 MPa, and 0.41 MPa, respectively. Therefore, only when the reservoir pressure reduced to 1.09 MPa, the coal seam can enter the fast desorption stage and further reach the sensitive desorption stage when pressure <0.41 MPa. The correlation between pressure nodes and coal rank is shown in Fig. 7(a). The change trend of three pressure nodes with increasing coal rank is similar with that of V_L and P_L, indicating that high rank coals are easier to reach the high CBM desorption efficiency and have inherent advantages in achieving high productivity. The relevant relationships between the R_o, the starting pressure (P_i), the turning pressure (P_t) and the sensitive pressure (P_s) are as follows:

$$P_i = -0.6982R_o^2 + 6.3897R_o - 3.6731 \quad (0.98\% \leqslant R_o \leqslant 4.3\%) \quad R^2 = 0.9514, \tag{10}$$

$$P_t = -0.4642R_o^2 + 4.2999R_o - 2.5411 \quad (0.98\% \leqslant R_o \leqslant 4.3\%) \quad R^2 = 0.9519, \tag{11}$$

$$P_s = -0.2132R_o^2 + 2.0591R_o - 1.3272 \quad (0.98\% \leqslant R_o \leqslant 4.3\%) \quad R^2 = 0.9489. \tag{12}$$

Meanwhile, the differences between different pressure nodes also increase with the increase of R_o (Fig. 7(b)). For example, the sensitive, fast, and slow stages of coal with R_o of 0.98% cover a pressure range of 0.41 MPa, 0.68 MPa and 0.63 MPa, respectively. For R_o of 4.13%, the pressure ranges of the sensitive, fast, and slow stages raise to 3.66 MPa, 3.74 MPa, and 3.5 MPa, respectively. Therefore, under the same conditions, CBM in lower rank coals is more difficult to reach the starting pressure than that in the higher rank coals. Once the pressure drops to

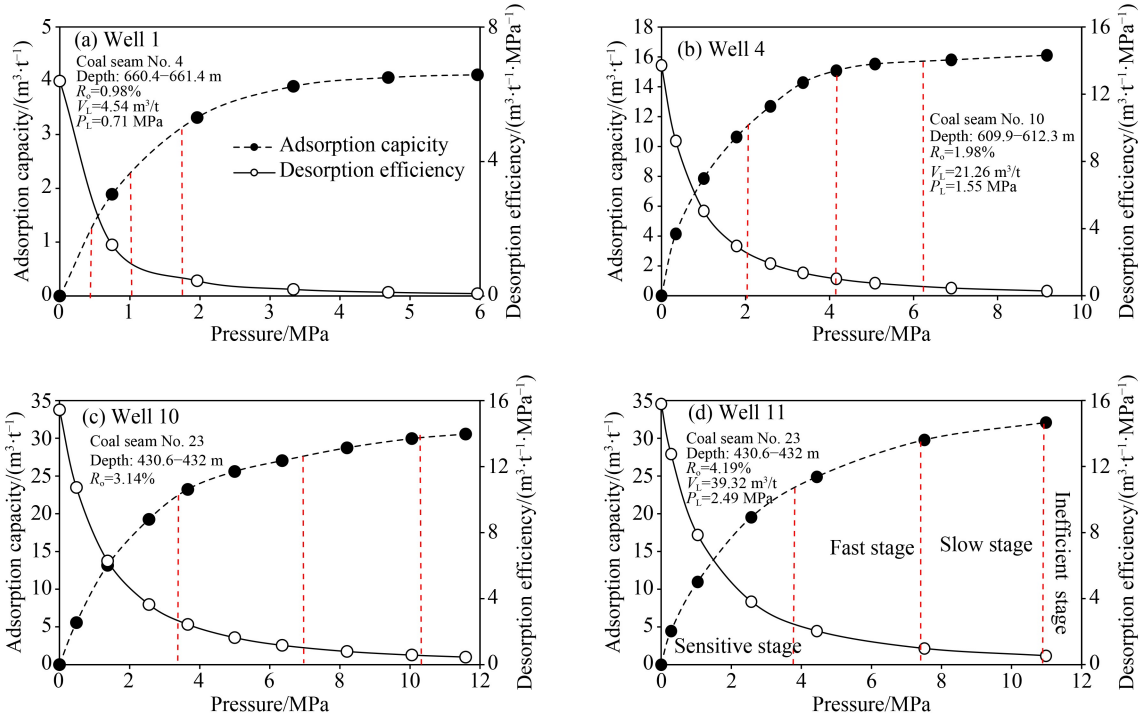

Fig. 6 The division of desorption stages of 4 typical coal samples.

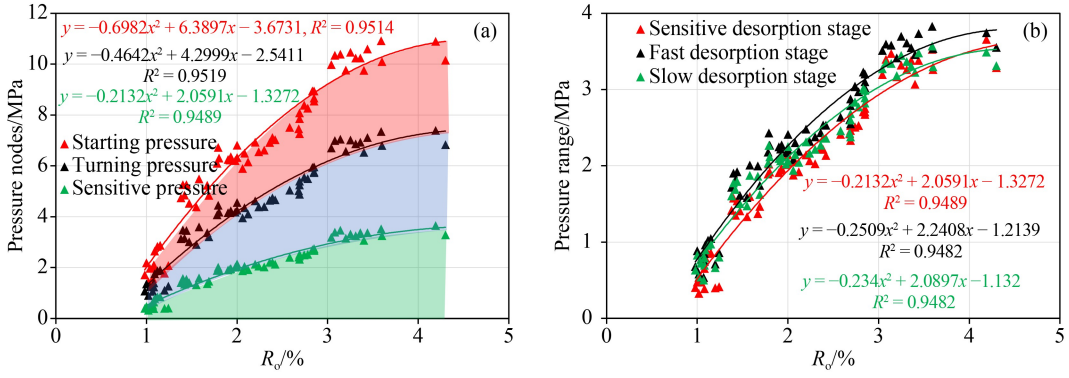

Fig. 7 (a) Correlations between the R_o, the starting pressure, the turning pressure and the sensitive pressure. (b) Pressure range of different desorption stages varies with increasing coal rank.

the starting pressure, it will reach the fast or sensitive desorption stages in a shorter time, which may be manifested by the rapid growth of gas production of CBM wells. However, it cannot maintain stable high gas rate for a long time because it will get close to the abandonment pressure faster. Here, abandonment pressure refers to the pressure at which economic production can no longer be sustained, which is one of the main indicators for calculating the maximum CBM recovery (Thakur et al., 2014). The abandonment pressure is about 0.7 MPa for CBM development in America, while that is between 0.2 and 1.0 MPa in China.

4.3 The desorption stages at early production process

In theory, the three pressure nodes will appear in any desorption process. However, CBM reservoirs have experienced partial desorption stages in the long geological history. Therefore, most CBM wells will not experience all four desorption stages due to differences in the critical desorption pressure caused by different Langmuir volume, Langmuir pressure, and gas content. The critical desorption pressure of CBM refers to the reservoir pressure corresponding to the desorption and adsorption behaviors reaching equilibrium, that is, the pressure at which the CBM adsorbed on the internal pore surface of coals begins to desorb. When the reservoir pressure drops below the critical desorption pressure, the gas desorbs, diffuses, and eventually flows into the wellbore. The critical desorption pressure (P_{cd}) can be calculated by Eq. (13) (Langmuir, 1916):

$$P_{cd} = \frac{V_m P_L}{V_L - V_m}. \quad (13)$$

Taking Eq. (8) and Eq. (9) into Eq. (13). The critical

desorption pressure can be expressed as a function related to R_o and V_m:

$$P_{cd} = \frac{V_m(-0.1988R_o^2 + 1.6206R_o - 0.6662)}{-2.017R_o^2 + 20.55R_o - 12.841 - V_m}, \quad (0.98\% \leqslant R_o \leqslant 4.3\%). \tag{14}$$

Under undersaturated reservoirs ($V_m \leqslant V_L$), the theoretical chart of the critical desorption pressure of different rank coals varies with the change in measured gas content is shown in Fig. 8. As the measured gas content increases, the coals show an upward trend in critical desorption pressure due to increased gas saturation. For the same gas content, the lower rank coals have the higher critical desorption pressure. Normally, the reservoir pressure is greater than the critical desorption pressure, and thus, there will be a single-water drainage stage in the CBM production process to achieve depressurization. The pressure differences between the reservoir pressure and the critical desorption pressure reflects the amount of pressure reduction required before the gas production, and guides the establishment of the CBM drainage control system. Otherwise, if the reservoir pressure is lower than the critical desorption pressure, the gas will desorb immediately, even if the coal reservoir may have a low gas content. In this case, the difference between the reservoir pressure and the abandonment pressure is generally small, indicating a shorter production cycle.

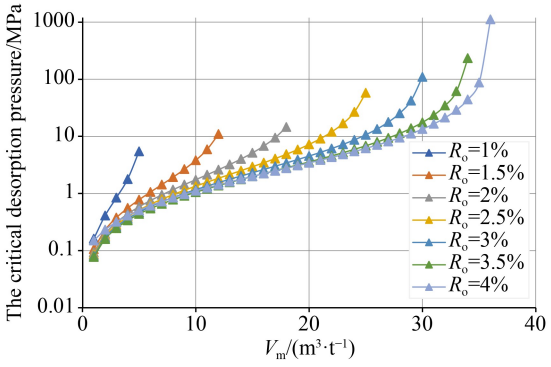

Fig. 8 The theoretical chart of the critical desorption pressure of different rank coals varies with measured gas content under undersaturated conditions ($V_m \leqslant V_L$).

Combining the Eq. (10), Eq. (11), Eq. (12), and Eq. (14), the theoretical chart of the critical desorption pressure of different rank coals and its relationships with the starting, turning and sensitive pressures are shown in Fig. 9. It can be seen that under the same gas content conditions, the higher the coal rank, the less desorption stages that CBM needs to go through. At the early production stage, the corresponding desorption efficiency at the critical desorption pressure can be used to reflect the CBM production and productivity. Taking CBM wells in the Bide syncline (well A; R_o,1.8%–2.5%) and the Zhuzang syncline (well B; R_o, 3.4%–4.0%) as examples (Fig. 10), and according to the CH_4 adsorption isotherm, the starting, turning, and the sensitive pressures of coal seam No. 32 in well A are 6.8 MPa, 4.5 MPa, and 2.1 MPa, respectively. For well B, the starting, turning, and the sensitive pressures of coal seam No. 23 are 10.6 MPa, 7.1 MPa, and 3.4 MPa, respectively. The critical desorption pressure of Well A is 2.66 MPa, which is located in the sensitive desorption stage. After the CBM is desorbed, as the BHFP decreases, the gas production increases rapidly. However, the critical desorption pressure of Well B is located in the slow desorption stage, and the gas production increase slowly at the early production phases. When the pressure drops to the turning pressure, the gas growth rate tends to increase. Generally, the higher desorption efficiency at early stage is conductive for high gas production. On the one hand, the higher desorption efficiency allows the coal seam to desorb a large amount of gas in a shorter time; on the other hand, the higher desorption efficiency can enhance

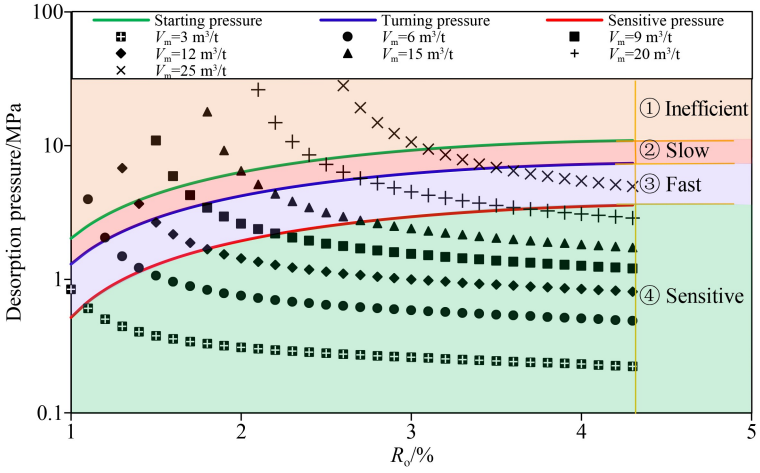

Fig. 9 The theoretical chart of the correlations between the critical desorption, starting, turning and sensitive pressures in undersaturated conditions ($V_m \leqslant V_L$).

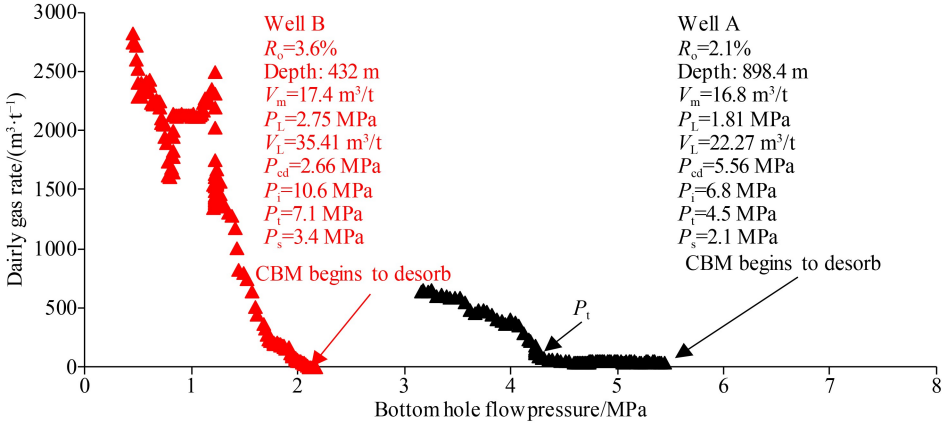

Fig. 10 Correlations between BHFP and daily gas rate of Well A and Well B at the early production stage.

the coal matrix shrinkage effect and increase the desorption area, thereby increasing the dynamic permeability (Harpalani and Schraufnagel, 1990; Mazumder et al., 2012; Connell et al., 2016; Pan and Connell, 2007).

4.4 Implication for CBM co-production from multiple coal seams

CBM is mainly stored in the coal seam in the state of adsorption, and its current development is generally based on the mechanism of "drainage → depressurization → gas desorption → diffusion → seepage → output". Different from the gas production from single-layer coal seam, the commingled layers will desorb in sequence during the gas co-production process from multiple coal seams (Fig. 11). With the production of formation water, the reservoir pressure and WLL height will decrease gradually. Once the reservoir pressure of upper coal seam reduces to the critical desorption, the CBM begins to desorb. Then, the lower coal seam reaches the critical desorption pressure and starts to desorb. With the continuous production, the WLL height will gradually drop below the depth of each layer, and the gas production rate will decrease sharply. This phenomenon has been proved by production practice. As shown in Fig. 12, a typical well selected No. 20, No. 23, No. 27, and No. 30 coal seams as the target layers for CBM co-production. With the decrease of the BHFP, the coal seams tend to desorb, and the gas production rate reaches the maximum value of 2021 m³/d in about 600 days. But at the same time, all producing coal seams tend to be lower than the WLL, and the most notable feature is that the casing pressure is equal to the BHFP. Therefore, the gas production rate gradually decreases as production continues.

Currently, the selection of commingled layers mainly focuses on whether the coal seam can desorb before the exposure. For example, Yang et al., (2018b) suggested that it should be ensured that the main gas production layer desorbs first and will not be exposed too early. Once the production layer is exposed, the damage to the gas production is irreversible (Zhang et al., 2014; Zhou et al., 2016). However, most of these studies ignored the important role of CBM desorption efficiency in different stages during production process. If the reservoir pressure of production layers still in an inefficient or slow desorption stage even after exposure, this layer will have very little contribution to total gas production with the overall productivity of "1 + 1 < 2". Therefore, in order to achieve the maximum production, it must be ensured that

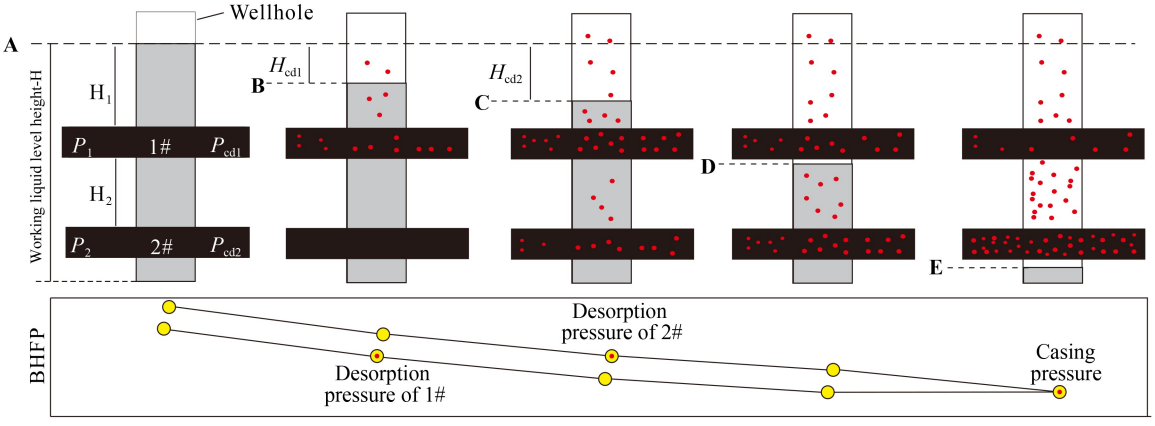

Fig. 11 Schematic diagram of production stages during multiple coal seams co-production process.

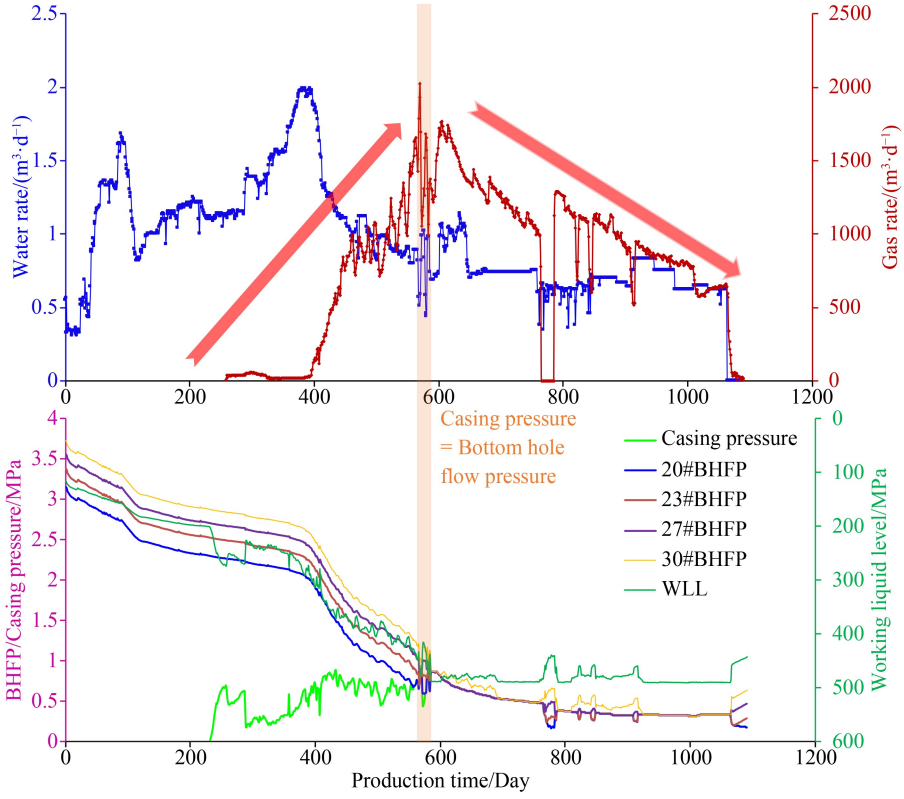

Fig. 12 A typical co-production CBM wells from the Zhuzang syncline

each production layer enters at least the fast desorption stage prior to exposure.

Except for varies coal rank distribution, the pressure and gas-bearing systems are vertically superposed in multiple coal seams, resulting in more complicated CBM geological conditions. Due to lack of fluid connectivity between different formation units, each unit has unique reservoir pressure and gas content conditions (Shen et al., 2016; Chen et al., 2018; Men et al., 2021; Men et al., 2021). Within the same system, the reservoir pressure and gas content increase gradually with increasing depth. The sudden change in the pressure coefficient can be considered as the boundary of different pressure systems. Taking well 3 in the Tucheng syncline as an example (Fig. 13), coal seams Nos. 1 + 3→No. 12 are within the same pressure system, and gas content increases with depth. For coal seams No. 13→No. 29, the pressure coefficient changes from 1.06 MPa/100 m to 1.4 MPa/100 m, and another increase trend in gas content is observed. The vertically superposed pressure is very common in the western Guizhou Province. At present, it was believed that water barriers with low permeability caused by both the sequence stratigraphic framework and tectonic stress are the main reasons for the formation of different pressure systems. In this case, different coal seams have different reservoir pressure, the critical desorption pressure will go through different desorption stages based on the Section 4.3. Also, the pressure difference between the reservoir pressure and the critical desorption pressure

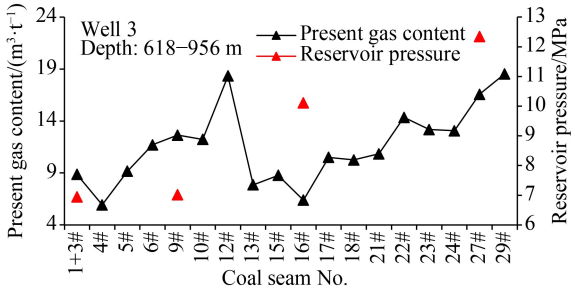

Fig. 13 The relationship between gas content and well test reservoir pressure of different coal seams in Well 3.

varies greatly, suggesting that the pressures-reduction required for achieving CBM desorption in different coal seams is different.

During CBM production process, it is difficult to monitor the gas and water production data of each production layer. The WLL height, the reservoir pressure, the critical desorption pressure, the desorption efficiency, and the division of the desorption stages can be used to reflect the CBM productivity in each layer, thus further determining whether different coal seams can produce gas by the same wellbore. The constraint is that fast desorption stages can be achieved in each seam before exposure. Here, we assume that the depth, reservoir pressure, the critical desorption pressure, and the turning pressure of coal seam No. x are h_x, P_x, P_{cdx}, and P_{tx}, respectively. The initial WLL of the lowermost coal seam

of CBM well is defined as H, which can be read by the contour map and topographic map. The h_x can be obtained through drilling data. The P_x is always measured by using the injection/fall-off well test. However, well test data for all seams is difficult to acquire, and only part of the coal seam is tested. Therefore, the P_x can be predicted based on statistical results of reservoir pressure and depth, following the work by Chen et al. (2019). The P_{cdx} and P_{tx} can be estimated by Fig. 9 if there is no isothermal adsorption curve. The P_{dx} is defined as the difference between the P_x and P_{cdx}, representing the required pressures-reduction for achieving desorption:

$$P_{dx} = P_x - P_{cdx}. \tag{15}$$

The height (H_x) between the WLL and the depth of coal seam No. x can be obtained from the difference between the depth of the coal seam No. x and the lowermost coal seam (h_L):

$$H_x = H - (h_L - h_x). \tag{16}$$

The pressure gradient (P_g) of hydrostatic column is about 1 MPa/100 m. Therefore, the relationship between the dynamic reservoir pressure (P_{drx}) and the dynamic wording liquid level height (H_{drx}) is as follows:

$$P_{drx} = \mathrm{P}_x - P_g \times (\mathrm{H}_x - \mathrm{H}_{drx}). \tag{17}$$

When the $P_{drx} = P_{cdx}$ and the H_{drx} is greater than h_x, the coal seam No. x begins to desorb:

$$\begin{cases} P_{drx} = P_{cdx} \\ \mathrm{H}_{drx} > h_x \end{cases}. \tag{18}$$

The above content only considers whether there is desorption or not, regardless of the contribution of gas production. Here, the P_{drx} is further defined as the difference between the P_x and P_{tx}, representing the required pressures-reduction from the reservoir pressure:

$$P_{dtx} = P_x - P_{tx}. \tag{19}$$

Therefore, only when $P_{drx} = P_{dtx}$ and the H_{drx} is greater than coal depth, the production layer can enter the fast desorption stage and reach the high desorption efficiency:

$$\begin{cases} P_{dtx} = P_{cdx} \\ \mathrm{H}_{drx} > h_x \end{cases}. \tag{20}$$

The above method is only analyzed from the perspective of desorption. In the actual production process, factors such as the gas content, the coal seam spacing (the depth difference between the top seam and the bottom seam), the abandonment pressure, the reservoir pressure difference, and the coal permeability should also be considered (Qin et al., 2018b; Yang et al., 2018a). The large reservoir pressure difference between different coal seams may cause interlayer interference, and the low gas content always means that a small amount of CBM can be desorbed from coal matrix. At present, coal seam spacing ⩽ 60 m is widely considered reasonable in China. However, according to this work, the coal space should depend on the relationship between the critical desorption pressure, the turning pressure, the reservoir pressure and the WLL. The permeability mainly refers to the seepage capacity of coal after artificial hydraulic fracturing and it changes with pressure (Tan et al., 2019). Separate layer fracturing is suggested to ensure all production layers can be fractured effectively.

5 Conclusions

1) The lower rank coals have lower values of V_L and P_L, while the higher rank coals exhibit strong adsorption capacity. As the pressure decreases, the CBM desorption efficiency increases exponentially. Under the same pressure conditions, the desorption efficiency of higher rank coals is greater than the lower rank coals, especially in the low-pressure zone.

2) The starting, turning, and sensitive pressures of higher rank coals are less than that of the lower rank coals, which are easier to reach the high CBM desorption efficiency and have inherent advantages in achieving high productivity.

3) Under the same conditions, the higher the coal rank, the less desorption stages that CBM needs to go through. At the early production stage, the corresponding desorption stage at the critical desorption pressure can reflect the CBM productivity, and fast/sensitive stages are key to achieve high gas production.

4) Multiple coal seams co-production is the best mode for CBM development in multi- and thin- coal seams. To achieve the maximum production, it is essential that production layers can enter at least the fast desorption stage and reach the high desorption efficiency prior to exposure. The WLL height, the reservoir pressure, the critical desorption pressure, the desorption efficiency, and the division of the desorption stages can be used to estimate whether different coal seams can produce gas by the same wellbore.

Acknowledgments This work was supported by the National Natural Science Foundation of China (Grant Nos. 42130802, 41772132), the Major Projects of Ningxia Key Research and Development Plan (No. 2020BFG2003), the Fundamental Research Funds for the Central Universities (No. 2652019095) and the Key Technologies R&D Programme of PetroChina Company Limited (No. 2021DJ2306). The authors are grateful to anonymous reviewers for their careful reviews and detailed comments, which helped to substantially improve the manuscript.

References

Beaton A, Langenberg W, Pană C (2006). Coalbed methane resources and reservoir characteristics from the Alberta Plains, Canada. Int J Coal Geol, 65(1−2): 93–113

Chen S, Tang D, Tao S, Ji X, Xu H (2019). Fractal analysis of the

dynamic variation in pore-fracture systems under the action of stress using a low-field NMR relaxation method: an experimental study of coals from western Guizhou in China. J Petrol Sci Eng, 173: 617–629

Chen S, Tang D, Tao S, Xu H, Zhao J, Fu H, Ren P (2018). *In-situ* stress, stress-dependent permeability, pore pressure and gas-bearing system in multiple coal seams in the Panguan area, western Guizhou, China. J Nat Gas Sci Eng, 49: 110–122

Chen S, Tao S, Tang D, Xu H, Li S, Zhao J, Jiang Q, Yang H (2017). Pore structure characterization of different rank coals using N_2 and CO_2 adsorption and its effect on CH_4 adsorption capacity: a case in Panguan syncline, western Guizhou, China. Energy Fuels, 31(6): 6034–6044

Chen S, Tao S, Tian W, Tang D, Zhang B, Liu P (2021a). Hydrogeological control on the accumulation and production of coalbed methane in the Anze Block, southern Qinshui Basin, China. J Petrol Sci Eng, 198: 108138

Chen S, Liu P, Tang D, Tao S, Zhang T (2021b). Identification of thin-layer coal texture using geophysical logging data: investigation by wavelet transform and linear discrimination analysis. Int J Coal Geol, 239: 103727

Chen S, Tang D, Tao S, Liu P, Mathews J P (2021c). Implications of the *in situ* stress distribution for coalbed methane zonation and hydraulic fracturing in multiple seams, western Guizhou, China. J Petrol Sci Eng, 204: 108755

Connell L D, Mazumder S, Sander R, Camilleri M, Pan Z, Heryanto D (2016). Laboratory characterisation of coal matrix shrinkage, cleat compressibility and the geomechanical properties determining reservoir permeability. Fuel, 165: 499–512

Crosdale P J, Beamish B B, Valix M (1998). Coalbed methane sorption related to coal composition. Int J Coal Geol, 35(1−4): 147–158

Dai S, Chou C L, Yue M, Luo K, Ren D (2005). Mineralogy and geochemistry of a Late Permian coal in the Dafang Coalfield, Guizhou, China: influence from siliceous and iron-rich calcic hydrothermal fluids. Int J Coal Geol, 61(3−4): 241–258

Department of Applied Mathematics in Tongji University (2002). Higher mathematics. Beijing: Higher Education Press

Harpalani S, Schraufnagel R A (1990). Shrinkage of coal matrix with release of gas and its impact on permeability of coal. Fuel, 69(5): 551–556

Langmuir I (1916). The constitution and fundamental properties of solids and liquids. J Am Chem Soc, 38(11): 2221–2295

Li Y, Zhang C, Tang D, Gan Q, Niu X, Wang K, Shen R (2017). Coal pore size distributions controlled by the coalification process: an experimental study of coals from the Junggar, Ordos and Qinshui basins in China. Fuel, 206: 352–363

Li Y, Yang J, Pan Z, Meng S, Wang K, Niu X (2019). Unconventional natural gas accumulations in stacked deposits: a discussion of upper Paleozoic coal-bearing strata in the east margin of the Ordos Basin, China. Acta Geol Sin (English Ed), 93(1): 111–129

Mazumder S, Scott M, Jiang J (2012). Permeability increase in Bowen Basin coal as a result of matrix shrinkage during primary depletion. Int J Coal Geol, 96: 109–119

Men X Y, Tao S, Liu Z X, Tian W G, Chen S D (2021). Experimental study on gas mass transfer process in a heterogeneous coal reservoir. Fuel Process Technol, 216: 106779

Meng Y, Tang D, Xu H, Qu Y L Y, Zhang W (2014). Division of coalbed methane desorption stages and its significance. Pet Explor Dev, 41(5): 671–677

Meng Y, Tang D, Xu H, Qu Y, Xu H, Li Y (2015). Division of the stages of coalbed methane desorption based on the Langmuir adsorption isotherm. Arab J Geosci, 8(1): 57–65

Mohanty D, Chattaraj S, Singh A K (2018). Influence of coal composition and maturity on methane storage capacity of coals of Raniganj Coalfield, India. Int J Coal Geol, 196: 1–8

Nie B, Liu X, Yang L, Meng J, Li X (2015). Pore structure characterization of different rank coals using gas adsorption and scanning electron microscopy. Fuel, 158: 908–917

Pan Z, Connell L D (2007). A theoretical model for gas adsorption-induced coal swelling. Int J Coal Geol, 69(4): 243–252

Qin Y, Moore T A, Shen J, Yang Z B, Shen Y L, Wang G (2018a). Resources and geology of coalbed methane in China: a review. Int Geol Rev, 60(5−6): 777–812

Qin Y, Wu J, Shen J, Yang Z, Shen Y, Zhang B (2018b). Frontier research of geological technology for coal measure gas joint-mining. J China Coal Soc, 43: 1504−1516 (in Chinese)

Qin Y, Xiong M, Yi T, Yang Z, Wu C (2008). On unattached multiple superposed coalbed methane system: in a case of the Shuigonghe syncline, Zhijin-Nayong Coalfield, Guizhou. Geol Rev, 54: 65−70 (in Chinese)

Ren P, Xu H, Tang D, Li Y, Sun C, Tao S, Li S, Xin F, Cao L (2018). The identification of coal texture in different rank coal reservoirs by using geophysical logging data in northwest Guizhou, China: investigation by principal component analysis. Fuel, 230: 258–265

Shen Y, Qin Y, Guo Y, Yi T, Yuan X, Shao Y (2016). Characteristics and sedimentary control of a coalbed methane-bearing system in Longtan (late Permian) coal-bearing strata of western Guizhou Province. J Nat Gas Sci Eng, 33(11): 8–17

Tan Y, Pan Z, Feng X T, Zhang D, Connell L D, Li S (2019). Laboratory characterization of fracture compressibility for coal and shale gas reservoir rocks: a review. Int J Coal Geol, 204: 1–17

Tao S, Pan Z J, Tang S L, Chen S D (2019a). Current status and geological conditions for the applicability of CBM drilling technologies in China: a review. Int J Coal Geol, 202: 95–108

Tao S, Chen S D, Pan Z J (2019b). Current status, challenges, and policy suggestions for coalbed methane industry development in China: a review. Energ Sci Eng, 7(4): 1059–1065

Tao S, Chen S D, Tang D Z, Zhao X, Xu H, Li S (2018). Material composition, pore structure and adsorption capacity of low-rank coals around the first coalification jump: a case of eastern Junggar Basin, China. Fuel, 211: 804–815

Thakur P, Schatzel S, Aminian K (2014). Coal Bed Methane: from Prospect to Pipeline. New York: Elsevier

Wang Z, Qin Y (2019). Physical experiments of CBM coproduction: a case study in Laochang district, Yunnan Province, China. Fuel, 239: 964–981

Wu S, Tang D, Li S, Wu H, Hu X, Zhu X (2017). Effects of geological pressure and temperature on permeability behaviors of middle-low volatile bituminous coals in eastern Ordos Basin, China. J Petrol Sci Eng, 153: 372–384

Wu Y, Pan Z, Zhang D, Lu Z, Connell L D (2018). Evaluation of gas production from multiple coal seams: a simulation study and economics. Int J Min Sci Technol, 28(3): 359–371

Wu Y L, Tao S, Tian W G, Chen H, Chen S D (2021). Advantageous seepage channel in coal seam and its effects on the distribution of high-yield areas in the Fanzhuang CBM Block, southern Qinshui Basin, China. Nat Resour Res, 30(3): 2361–2376

Xu W, Li J, Wu X, Liu D, Wang Z (2021). Desorption hysteresis of coalbed methane and its controlling factors: a brief review. Front Earth Sci, 15(2): 224–236

Xu H, Sang S, Yang J, Jin J, Hu Y, Liu H, Li J, Zhou X, Ren B (2016). Selection of suitable engineering modes for CBM development in zones with multiple coalbeds: a case study in western Guizhou Province, southwest China. J Nat Gas Sci Eng, 36: 1264–1275

Yang Z, Qin Y, Yi T, Tang J, Zhang Z, Wu C (2018b). Analysis of multi-coalbed CBM development methods in western Guizhou, China. Geosci J, 23: 1–11

Yang Z, Zhang Z, Qin Y, Wu C, Yi T, Li Y, Tang J, Chen J (2018a). Optimization methods of production layer combination for coalbed methane development in multi-coal seams. Pet Explor Dev, 45(2): 312–320

Zhang C, Xu J, Peng S, Li Q, Yan F (2019). Experimental study of drainage radius considering borehole interaction based on 3D monitoring of gas pressure in coal. Fuel, 239: 955–963

Zhang Z, Qin Y, Fu X H (2014). The favorable developing geological conditions for CBM multi-layer drainage in southern Qinshui Basin. J China Univ Min Technol, 43: 1019–1024

Zhao S, Wang Y, Li Y, Wu X, Hu Y, Ni X, Liu D (2021). Co-production of tight gas and coalbed methane from single wellbore: a simulation study from northeastern Ordos Basin, China. Nat Resour Res, 30(2): 1597–1612

Zhao J, Xu H, Tang D, Mathews J P, Li S, Tao S (2016). A comparative evaluation of coal specific surface area by CO_2, and N_2, adsorption and its influence on CH_4, adsorption capacity at different pore sizes. Fuel, 183: 420–431

Zhou X, Sang S, Yi T, Jin J, Huang H, Hou D, Ao X (2016). Damage mechanism of upper exposed producing layers during CBM multi-coal seam development. Nat Gas Ind, 36: 52–59